



Full Text View

[Volume 30, Issue 11 \(November 2000\)](#)

Journal of Physical Oceanography

Article: pp. 2972–2988 | [Abstract](#) | [PDF \(1.06M\)](#)

Coupled Rossby Waves in the Indian Ocean on Interannual Timescales

Warren B. White

Scripps Institution of Oceanography, University of California, San Diego, La Jolla, California

(Manuscript received June 2, 1999, in final form February 1, 2000)

DOI: 10.1175/1520-0485(2001)031<2972:CRWITI>2.0.CO;2

ABSTRACT

Gridded fields of TOPEX/Poseidon sea level height (SLH) from 1993 to 1998 and National Centers for Environmental Prediction sea surface temperature (SST) and meridional surface wind (MSW) anomalies from 1970 to 1998 are used to examine coupled Rossby waves in the Indian Ocean from 10°S to 30°S. Time–longitude diagrams of monthly SLH, SST, and MSW anomalies yield significant peak spectral energy density in propagation wavenumber–frequency spectra for westward propagating waves of >2 yr period and >4000 km wavelength. Subsequent low-pass filtering of SLH, SST, and MSW anomalies for these interannual timescales >2 yr finds them propagating westward over the Indian Ocean in fixed phase with one another at speeds significantly less ($0.04\text{--}0.07\text{ m s}^{-1}$) than first-mode baroclinic Rossby waves, taking 3 to 4 years to cross the basin. These coupled Rossby waves display weak beta refraction patterns in all three variables. Significant squared coherence between interannual SLH and SST (SST and MSW) anomalies yield phase differences ranging from 0° to 45° (150° to 180°). Warm SST anomalies overlie high SLH anomalies, suggesting that pycnocline depth anomalies associated with the Rossby waves modify vertical mixing processes to maintain SST anomalies against dissipation. Warm SST anomalies are associated with outgoing latent heat flux anomalies in the eastern and central ocean, indicating that the ocean is capable of forcing the overlying atmosphere. Poleward MSW anomalies occur directly over warm SST anomalies, suggesting that anomalous planetary vorticity advection balances anomalous low-level convergence in response to SST-induced midtroposphere convection. These inferred thermodynamic processes allow a simple analytical model of coupled Rossby waves to be constructed that yields much slower westward phase speeds than for free Rossby waves, as observed. Maintenance of wave amplitude against dissipation occurs for coupled waves that travel westward and poleward, as observed.

Table of Contents:

- [Introduction](#)
- [Data and methods](#)
- [Zonal wavenumber–frequency](#)
- [Time–longitude](#)
- [Westward phase speeds](#)
- [Phase relationships between](#)
- [Spatial refraction patterns](#)
- [Coupled Rossby waves](#)
- [A simple analytic model](#)
- [Discussion and conclusions](#)
- [REFERENCES](#)
- [APPENDIX](#)
- [FIGURES](#)

Options:

- [Create Reference](#)
- [Email this Article](#)
- [Add to MyArchive](#)
- [Search AMS Glossary](#)

Search CrossRef for:

- [Articles Citing This Article](#)


Search Google Scholar for:

- [Warren B. White](#)

1. Introduction


[Masumoto and Meyers \(1998\)](#) observed interannual Rossby waves with periods ranging from 3 to 5 yr in the tropical Indian Ocean from 6° to 14°S for 10 years from 1984 to 1993 in anomalous depth of the 20°C isotherm. This was made possible by expendable bathythermograph temperature profiles made along repeated sections by volunteer observing ships transiting the Indian Ocean. These interannual Rossby waves were not generated at the west coasts of Indonesia and Australia, but were forced by wind stress curl anomalies in the interior ocean along Rossby wave ray paths. [Masumoto and Meyers \(1998\)](#) found these wind-forced interannual Rossby waves superimposed upon a zonal standing wave component in the tropical Indian Ocean on these 3–5 yr period scales, with thermocline depth anomalies in the eastern ocean fluctuating out of phase with those in the western ocean, making detection of the propagating Rossby waves more difficult.

[Perigaud and Delecluse \(1993\)](#) observed interannual Rossby waves with periods ranging from 3 to 4 yr in the Indian Ocean near 15°S for 5 years from 1985 to 1989 in anomalous sea level height (SLH). This was made possible from the analysis of Geosat satellite altimeter data made along repeated tracks over the Indian Ocean. These interannual Rossby waves propagated slower than those simulated in a wind-forced Rossby wave model (see their Fig. 7) but at about the same speed as westward propagating wind stress curl (WSC) anomalies. Both SLH and WSC anomalies took 2–3 years to propagate westward across the Indian Ocean at 15°S. [Perigaud and Delecluse \(1993\)](#) had difficulty reconciling these observations with model results, concluding that uncertainties in the anomalous WSC forcing would not allow the model to simulate the observed Rossby waves.


In the present study we examine ocean–atmosphere coupling of oceanic Rossby waves in the Indian Ocean from 10°S to 30°S ([Fig. 1](#) ) on interannual timescales ranging in period from 2 to 5 yr. We begin by examining westward phase propagation between covarying SLH, SST, and meridional surface wind (MSW) anomalies for the period of the TOPEX/Poseidon altimetry from 1993 to 1998. We determine the phase relationships between these three variables, limiting the possible thermodynamical mechanisms responsible for coupling. This allows us to construct a simple analytic coupled model that provides insight into the dispersion relationship for coupled Rossby waves. To gain statistical confidence in these results we also examine westward phase propagation in covarying SST and MSW anomalies for 29 years from 1970 to 1998 in the National Centers for Environmental Research (NCEP) reanalysis ([Kalnay et al. 1996](#)).

2. Data and methods

We utilize gridded SLH data over the global ocean for 6 years from January 1993 to December 1998 available from the T–P altimeter, analyzed by A. Hayashi, V. Zlotnicki, and L. Fu (1998, personal communication). These SLH data, initially on discrete ground tracks laid down over the globe and repeated nominally every 10 days, were interpolated onto a 1° lat × 1° long grid from approximately 60°S to 60°N on the middle of each month. We analyze these monthly T–P SLH data over the tropical Pacific basin ocean together with the NCEP SST data ([Reynolds and Marsico 1993](#)) and MSW data ([Kalnay et al. 1996](#)). The NCEP data are on an approximate 2° lat × 2° long grid over the global ocean, with SST data available biweekly and MSW data available twice daily for the 29 years from 1970 to 1998. Prior to analysis we interpolated all three datasets to a standard 2° lat × 2° long grid at the middle of each month. This yields 72-month time sequences from 1993 to 1998 for SLH, SST, and MSW data, and 29-yr time sequences from 1970 to 1998 for SST and MSW data. Next we compute 6-yr (29-yr) long-term monthly means at each grid point and subtract them from individual monthly means, yielding time sequences of monthly anomalies about the mean annual cycle at each grid point for the 72 months (29 years) from January 1993 to December 1998 (1970–98).

In the present study, we examine SLH, SST, and MSW anomalies from 10°S to 30°S in the Indian Ocean from 1993 to 1998, but we focus on 10°, 14°, 18°, 22°, and 26° latitudes ([Fig. 1](#) ). Peak spectral energy density in zonal wavenumber frequency spectra computed along these latitudes (not shown) occurs for period scales >2 yr; so we temporally filter these 72-month time sequences to examine interannual anomalies for periods greater than 2 yr (see appendix), yielding 60-month time sequences of interannual anomalies extending from June 1993 to May 1998. We remove the zonal mean and a trend across the Indian Ocean at each latitude to enhance the zonal wave propagation. Later we examine interannual SST and MSW anomalies over the same latitude domain for 29 years from 1970 to 1998, obtained by bandpass filtering monthly anomalies with half-power points at 24–84 months ([Kaylor 1977](#)).

3. Zonal wavenumber–frequency spectra

We begin by constructing zonal wavenumber–frequency spectra of interannual SLH anomalies along constant latitudes at 10°S, 14°S, 18°S, 22°S, and 26°S in the south Indian Ocean ([Jackson 1996](#), pp. 295–301). These are not shown but spectral energy density was much larger in the left-hand quadrant than in the right-hand quadrant, indicating a dominance of westward propagating waves over eastward propagating and standing waves. So we display the difference between spectral estimates in both quadrants yielding the “propagation” wavenumber–frequency spectrum ([von Storch and Zwiers 1999](#), 241–250). The absence of negative spectral energy density in these propagation spectra (left, [Fig. 2](#) ) is testament to the

dominance of westward propagation in interannual SLH anomalies. At each latitude these propagation spectra are red in both frequency and zonal wavenumber, with peak spectral energy density for periods >2 yr and zonal wavelengths >4000 km. We superimpose the free Rossby wave dispersion curve upon each spectra, yielding constant westward phase speeds in the long-wave limit computed by [Killworth et al. \(1997\)](#).

Propagation zonal wavenumber-frequency spectra for interannual SST and MSW anomalies (middle and right, [Fig. 2](#)) are very similar to those for interannual SLH anomalies (left, [Fig. 2](#)). These spectra yield spectral energy density for westward propagating waves at approximately the same periods and wavelengths; that is, >2 yr and >4000 km. So at each latitude, significant peak spectral energy density for all three variables are in close proximity to one another, with the center of shared spectral energy density estimated by the solid circle. Zonal wavenumbers and frequencies designated by this circle are displaced well to the left of the free Rossby wave dispersion curve, indicating slower speeds for the waves sharing westward phase propagation among the three variables.

4. Time–longitude diagrams of covarying SLH, SST, and MSW anomalies

The simulation of interannual Rossby waves in a time–longitude diagram of interannual pycnocline depth anomalies along 13°S by [Masumoto and Meyers \(1998\)](#) led them to hypothesize that observed Rossby waves at this latitude derived from anomalous WSC forcing by the overlying atmosphere. Here we examine time–longitude diagrams of interannual SLH, SST, and MSW anomalies (left, [Fig. 3](#)) used to compute propagation spectra at these latitudes ([Fig. 2](#)) and find the three variables covarying in their joint westward propagation over the 5-year time sequence from July 1993 to June 1998 (with 6 months deleted from both ends of the record due to low-pass temporal filtering, see appendix). A similar analysis conducted by [White \(2000\)](#) in the Pacific Ocean required zonal bandpass filtering to separate westward propagating Rossby waves from eastward propagating SST waves of global space scale; that is, the global ENSO wave observed propagating eastward across the global tropical ocean by [White and Cayan \(2000\)](#). But since the Indian Ocean extends over less longitude than the Pacific Ocean we need only remove the zonal mean and trend to isolate the basin-scale westward traveling Rossby waves from global-scale eastward propagating SST waves.

Representative time–longitude diagrams of interannual SLH, SST, and MSW anomalies at 10°S , 18°S , and 26°S in the Indian Ocean (left, [Fig. 3](#)) display westward phase propagation in these three variables. These variables covary in a manner consistent with biennial Rossby waves in the Pacific Ocean ([White 2000](#)) but with different phase relationships. In each time–longitude diagram (left, [Fig. 3](#)) we plot a dashed line along the zero line separating positive and negative anomalies of SLH. This is repeated in time–longitude diagrams for SST and MSW anomalies, allowing us to assess the degree of alignment among the three variables and to estimate their westward phase speeds and their respective phase relationships, the latter quantified below utilizing coherence and phase statistics.

At 10°S the dashed line marking the separation between negative and positive SLH anomalies nearly overlays the zero line separating negative from positive SST anomalies, and separating poleward from equatorward MSW anomalies (top left, [Fig. 3](#)). The alignment among the three variables indicates that Rossby waves in anomalous SLH are coupled to the overlying atmosphere through their influence upon SST anomalies. So warm SST anomalies overlying high SLH anomalies overlie downward displacements of the main pycnocline as well. This suggests that in the Indian Ocean vertical displacements in the pycnocline associated with Rossby waves play a dominant role in specifying the phase relationship between SLH and SST anomalies. Poleward MSW anomalies also overlie warm SST anomalies, consistent with planetary vorticity advection responding to stretching of the lower troposphere by SST-induced midtroposphere diabatic heating ([Palmer and Sun 1985](#)). Wave amplitude in SLH anomaly was approximately uniform in both time and space, indicating that coupled Rossby waves at 10°S were relatively stable as they propagated westward across the Indian Ocean.

At 18°S , SLH, SST, and MSW anomalies were again found to propagate westward together, with phase relationships the same as at 10°S (middle left, [Fig. 3](#)). At this latitude the wave amplitude in SLH anomaly was more intense in the eastern portion of domain and during the second half of the record when the alignment of the three variables was better. As observed in the Pacific Ocean ([White 2000](#)), the alignment (and presumed coupling) between ocean and atmosphere in the Indian Ocean appears to wax and wane in both time and space, yielding intense (weak) coupled Rossby waves in SLH anomaly when alignment among all three variables is strong (weak or absent).

At 26°S , SLH, SST, and MSW anomalies propagated westward together but with SST and MSW anomalies superimposed upon either standing or eastward propagating waves (bottom left, [Fig. 3](#)). Even so, the phase relationships among the three variables were similar to those at 18°S and 10°S . This indicates that coupling of oceanic Rossby waves to the overlying atmosphere in the Indian Ocean was similar across both the Tropics and extratropics. This is different from that observed in the Pacific Ocean where phase relationships between SST and MSW anomalies changed from the Tropics to extratropics ([White 2000](#)). In the Pacific Ocean SST and MSW anomalies are displaced by approximately 90° (0°) of phase in the Tropics (extratropics), while in the Indian Ocean they are displaced by approximately 0° of phase at all latitudes.

Examining the time–longitude diagrams together finds coupled Rossby wave activity more energetic in the Tropics than in the extratropics. Moreover greater competition between standing and traveling waves occurs in the higher latitudes. At each

latitude, covarying SLH, SST, and MSW anomalies took 3 to 4 years to propagate westward across the Indian Ocean; this is longer than the 2 to 3 years for SLH anomalies observed by [Perigaud and Delecluse \(1993\)](#) to cross the Indian Ocean in the late 1980s. We investigate this in more detail below.

5. Westward phase speeds of coupled Rossby waves

Speeds of westward phase propagation of coupled Rossby waves (right, [Fig. 3](#)) are estimated from the slopes of dashed lines in the time–longitude diagrams of covarying SLH, SST, and MSW anomalies (left, [Fig. 3](#)) for the period 1993–98, with error bars determined by possible changes in slope that could occur to accommodate errors in interannual SLH anomalies. These error bars capture westward phase speeds indicated by solid circles in zonal wavenumber–frequency spectra ([Fig. 2](#)), consistent with those choices for wavenumber and frequency of shared variance. Superimposed upon these observed phase speeds is the meridional profile of phase speed expected of free Rossby waves in the long-wave limit for the south Indian Ocean ([Killworth et al. 1997](#)).

At 10°S westward phase speeds (right, [Fig. 3](#)) are estimated from the slope of dashed lines in the time–longitude diagrams (left, [Fig. 3](#)) to be $-0.06 (\pm 0.03) \text{ m s}^{-1}$, approximately $\frac{1}{4}$ of the expected phase speed of free Rossby waves for the Indian Ocean. At 18°S westward phase speeds are estimated to be $0.05 \pm 0.03 \text{ m s}^{-1}$, only 20% smaller than at 10°S but approximately $\frac{1}{2}$ the expected speed of free waves for the Indian Ocean. At 26°S westward phase speeds are estimated to be $0.04 (\pm 0.03) \text{ m s}^{-1}$, significantly smaller than expected speeds of free waves for the Indian Ocean. These observed westward phase speeds are consistent with those estimated in [Fig. 2](#).

So the interannual coupled Rossby waves in the tropical Indian Ocean propagated westward much slower than free Rossby waves ([Killworth et al. 1997](#)) and slower than forced Rossby waves simulated in numerical ocean models by [Masumoto and Meyers \(1998\)](#). In the extratropics near 26°S the coupled and free wave speeds are nearly the same. The meridional profile of the observed westward phase speeds from 10° to 26° lat shows much smaller reduction in speed with latitude than for free waves, suggesting that the beta refraction pattern ([White 1977](#)) is much reduced in these coupled Rossby waves. This is confirmed below.

6. Phase relationships between covarying SLH, SST, and MSW anomalies

The dynamics of coupling between ocean and atmosphere responsible for coupled Rossby waves in the south Indian Ocean are reflected in temporal and spatial phase relationships between SLH, SST, and MSW anomalies ([White et al. 1998](#)). So we compute spectral coherence and phase ([Bendat and Piersol 1986](#), pp. 361–424) between interannual SLH and SST anomalies and interannual SST and MSW anomalies from 10°S to 26°S over the 6 years from January 1993 to December 1998 along thin lines displayed in [Fig. 1](#).

Squared coherence between interannual SLH and SST anomalies ranges from 0.8 to 0.9 from 10°S to 26°N, significant at the 90% confidence level at all latitudes, while phase differences range from 0° to 45°, each estimate significant at $\pm 30^\circ$ (Jenkins and Watts 1968, pp. 379–381). These average phase differences indicate that warm (cool) SST anomalies approximately overlie high (low) SLH anomalies, consistent with those observed in time–longitude diagrams (left, [Fig. 3](#)). As noted earlier this is a much different situation than 90° phase differences observed for biennial coupled Rossby waves in the Pacific Ocean ([White et al. 1998](#)).

Squared coherence between interannual SST and MSW anomalies ranges from 0.8 to 0.9 from 10°S to 26°S, significant at the 90% confidence level at all latitudes, while phase differences range from 150° to 180°, each estimate significant at $\pm 30^\circ$ (Jenkins and Watts 1968, pp. 379–381). This indicates that over the entire latitude domain poleward (equatorward) MSW anomalies occurred over warm (cool) SST anomalies, consistent with those observed in time–longitude diagrams (left, [Fig. 3](#)). These are also similar to that observed for extratropical coupled Rossby waves in the Pacific Ocean ([White et al. 1998](#); [White 2000](#)). The lack of a transition in phase difference from the Tropics to the extratropics separates the Indian Ocean from the Pacific Ocean, where in the Tropics the SST and MSW anomalies were displaced by approximately 90° of phase on biennial period scales ([White 2000](#)).

7. Spatial refraction patterns of coupled Rossby waves

Next we examine horizontal spatial patterns of coupled Rossby waves in the Indian Ocean. Free Rossby waves are characterized by a beta-refraction pattern with wave crests and troughs aligned so that the wave vector progressively points into the poleward direction with increasing longitude from the wave source (e.g., [White 1977](#)). This arises from wave refraction stemming from the decrease in westward phase speed with increasing latitude. In the meridional profile of coupled Rossby waves speeds (right, [Fig. 4](#)) the reduction in westward phase speed with latitude can be seen to have been much less than expected of free or forced Rossby waves. Thus we expect a much reduced refraction pattern. Moreover we expect the refraction pattern to appear in all three variables, as observed in [White et al. \(1998\)](#) and [White \(2000\)](#).

The animation sequences of maps for interannual SLH, SST, and MSW anomalies extending over the 6 years from January 1993 to December 1998 (Fig. 4) display westward phase propagation in all three variables over most of the record, with variables better aligned after January 1994 than before. After January 1995 crests and troughs in each variable were aligned in the northwest direction so that wavenumber vectors (normal to the crests and troughs) were directed westward and poleward. As this occurred after 1995 the amplitudes of all three variables became more robust and better aligned with one another than previously (i.e., better coupled). The phase relationships between variables can be ascertained from the dashed reference lines in Fig. 4 where we find warm (cool) SST anomalies approximately overlying high (low) SLH anomalies, and poleward (equatorward) MSW anomalies approximately overlying warm (cool) SST anomalies. These phase relationships are consistent with those determined by the coherence and phase analysis.

These results reveal two important aspects of coupled Rossby waves in the Indian Ocean on interannual timescales. First, they were more intensely coupled during the second half of the 6-yr record than during the first half as evidenced by a better alignment of the three variables and more intense amplitudes (Fig. 4). Second, they can be seen to have originated at the eastern boundary along the west coasts of Indonesia and Australia. The latter differs from observations of forced Rossby waves by Masumoto and Meyers (1998). These animation sequences suggest that Rossby waves at the west coasts of Indonesia and Australia were pumped by the anomalous MSW at these coasts as observed by White and Saur (1983) at the west coast of North America, but this remains to be demonstrated in coupled model simulations.

8. Coupled Rossby waves in covarying SST and MSW anomalies from 1970 to 1998

To this point we have only been able to construct a case study for interannual coupled Rossby waves through 1 to 2 cycles of variability over a 6-yr period. Next we establish the presence of coupled Rossby waves in the Indian Ocean prior to the availability of T-P satellite altimetry by inferring their presence in the westward propagation of covarying interannual NCEP SST and MSW anomalies across the Indian Ocean for 29 years from 1970 to 1998 (see section 2). This allows us to examine these interannual coupled Rossby waves over approximately eight cycles of variability.


To conduct this statistical study we apply complex empirical orthogonal function (CEOF) analysis to interannual SST and MSW anomalies over this period. CEOF analysis differs from EOF analysis by realizing propagating modes of variability in a time sequence of maps with a pair of real and imaginary components in quadrature with one another (Preisendorfer 1988). But propagating and standing waves of similar time and space scales linearly superimpose in a CEOF mode as they do in EOF modes. To partition propagating and standing waves in CEOF modes, White and Cayan (2000) confirmed the concept that propagating waves can be represented by the portion of shared variance between real and imaginary components while standing waves can be represented by their difference. This method necessarily yields standing and propagating waves that have identical patterns during some phase of respective standing and propagating wave activity.



So we apply CEOF analysis to interannual SST and MSW anomalies over the 29-yr record, yielding the dominant CEOF modes, displaying both the time sequence of the amplitudes and the animation sequences of their standing and propagating wave parts (Fig. 5). Dominant CEOF modes account for 51% (46%) of the interannual SST (SLP) variance over the 29 years. Here we find the two time sequences of the amplitudes (top, Fig. 5) overlying each other, correlated at 0.83 at zero phase lag over the 29 years. Major peaks in both modes occurred during 1970, 1973, 1975, 1977, 1979, 1982, 1987, 1989, 1991, 1995, and 1998, dominated by some combination of biennial variability and quadrennial variability. This indicates that interannual SST and MSW variability contained in these dominant CEOF modes covary with one another over the record.




When we partition propagating and standing waves in the first CEOF mode, we find the rms of standing wave variability in SST and MSW weights to be $0.04 (\pm 0.01) ^\circ\text{C}$ and $0.08 (\pm 0.02) \text{ m s}^{-1}$, respectively, while the rms of propagating wave variability is $0.025 (\pm 0.01) ^\circ\text{C}$ and $0.04 (\pm 0.01) \text{ m s}^{-1}$. So for both SST and MSW variability, amplitudes of standing waves were about twice those of propagating waves on average over the 29 years. These differences in amplitude can be seen in animation sequences of maps for standing and propagating wave weights (middle and bottom, Fig. 5). The animation sequence for the standing wave is constructed by multiplying the real CEOF spatial component by cosine of the phase, where its amplitude has been reduced by that portion of variance given to the propagating wave (White and Cayan 1999). The animation sequence for the propagating wave is constructed by multiplying real and imaginary CEOF spatial components by the cosine and sine of the phase, respectively, where their amplitudes have been reduced by that portion of the variance given to the standing wave (White and Cayan 2000). In this latter computation, real and imaginary components are weighted equally. Here maximum amplitude of the standing wave in SST can be seen to be approximately 0.1°C (middle left, Fig. 5), while that for the propagating wave is approximately 0.08°C (bottom left, Fig. 5). Maximum amplitude of the standing wave in MSW can be seen to be approximately 0.4 m s^{-1} (middle right, Fig. 5) while that for the propagating wave is approximately 0.2 m s^{-1} (bottom right, Fig. 5).

Animation sequences for the propagating wave in the first CEOF of SST and MSW anomalies (bottom, Fig. 5) display the same beta refraction patterns shown in animation sequences of SST and MSW anomalies (Fig. 4), with poleward


MSW overlying warm SST anomalies as observed earlier. So we see in these animation sequences that coupled Rossby waves were superimposed upon a standing wave in the Indian Ocean and with magnitudes only half as large. [Masumoto and Meyers \(1998\)](#) also found forced interannual Rossby waves superimposed upon a standing wave in the tropical Indian Ocean.

To determine whether SST and MSW are statistically correlated with each other over the 29-yr record, we plot time–longitude diagrams of interannual SST and MSW anomalies averaged along 16°S (top left, [Fig. 6](#) ). They show interannual SST and MSW anomalies propagating westward together from 1970 to 1977 and from 1982 to 1998, but not from 1978 to 1981. Even during periods of covariance the alignment of SST and MSW anomalies was better during some periods than during others. During the period from 1986 to 1990 [Perigaud and Delecluse \(1993\)](#) observed SLH and WSC anomalies taking 2 to 3 years to propagate across the Indian Ocean; we also find SST and MSW anomalies taking 2 to 3 years to propagate across the Indian Ocean, slower during later and earlier periods.

We also display time–longitude diagrams of SST and MSW anomalies reconstructed from the propagating wave part in the first CEOF of interannual variability (top right, [Fig. 6](#) ). They show coupled Rossby wave activity throughout most of the record, varying in amplitude, speed of propagation, and frequency. By comparing time–longitude diagrams with those of interannual anomalies themselves (left, [Fig. 6](#) ) we can observe when propagating waves dominated standing waves and vice versa.

We construct zonal lag cross-correlations between interannual and reconstructed SST and MSW anomalies over first and second halves of these time–longitude diagrams (bottom, [Fig. 6](#) ) finding them correlating significantly near zero zonal phase lag in all cases. Correlations are significantly higher for interannual anomalies reconstructed from the propagating wave part in the first CEOF mode (bottom right, [Fig. 6](#) ) than for interannual anomalies themselves (bottom left, [Fig. 6](#) ). In both cases results are consistent with coherence and phase relationships found between SST and MSW anomalies over the 6 years from 1993 to 1998 in [section 6](#).

9. A simple analytic model for coupled Rossby waves in the Indian Ocean

Simple analytic coupled models for extratropical and tropical coupled Rossby waves on biennial timescales have already been constructed by [White et al. \(1998\)](#) and [White \(2000\)](#). They computed westward phase speeds for coupled Rossby waves in the tropical Pacific Ocean of 0.10–0.15 m s^{−1}, less than those of free Rossby waves but not as small as those observed in the tropical Indian Ocean ranging from 0.04 to 0.07 m s^{−1} ([Fig. 4](#) ). So the tropical Indian Ocean contains coupled Rossby waves with westward phase speeds much smaller than those observed and simulated in the tropical Pacific Ocean. The reason for these differences may lie in the phase relationships between SLH and SST anomalies. Throughout the Pacific Ocean warm (cool) SST anomalies were found displaced approximately 90° of phase to the west of high (low) SLH anomalies (e.g., [White et al. 1998](#)) while throughout the Indian Ocean they were found approximately aligned. This different phase relationship indicates the existence of yet another class of coupled Rossby waves.

We now construct a simple analytic model for this new class of coupled Rossby waves, varying principally from the earlier model by the way SLH and SST anomalies are related. Thus we replace the anomalous upper-ocean heat budget in this latter study with the following idealized heat balance:

$$K_T T = (\bar{T}/\bar{H}) K_H h, \quad (9.1)$$

where h is the pycnocline depth anomaly, positive downward, associated with first mode baroclinic Rossby waves; T is the vertical-average temperature anomaly in the upper layer of the ocean above the main pycnocline, representing the SST anomaly; \bar{T} is the annual mean vertical-average temperature above the main pycnocline, representing the annual mean SST; \bar{H} is the annual mean depth of the main pycnocline; $K_T T$ parameterizes the anomalous heat loss from the upper ocean to the lower troposphere through sensible-plus-latent heat exchange during autumn–winter ([Frankignoul and Reynolds 1983](#)); and $K_H h$ parameterizes the anomalous heat gain by the upper ocean by reducing the entrainment of cold water into the near-surface mixed layer during autumn–winter through anomalous deepening of the main pycnocline ([Moisan and Niiler 1998](#)).

We set K_T^{-1} equal to 3 months, which is the e -folding scale time over which SST anomalies begin to dominate air temperature anomalies in the anomalous sensible-plus-latent heat exchange in the extratropics ([Kraus and Morrison 1966](#)).

We set K_H^{-1} equal to 6 months, which is the scale time over which pycnocline depth anomalies associated with interannual Rossby waves introduce an anomalous heat gain into the near-surface mixed layer over the autumn–winter season.

The assumption that latent heat flux anomalies are related to SST anomalies needs to be examined in the Indian Ocean. The bulk formula for latent heat flux anomalies has two contributions under perturbation expansion, the gradient-induced part based upon the air–sea specific humidity differences and the wind-induced part based upon the magnitude of the

anomalous wind and its direction with respect to the background wind. The question is not whether latent heat flux anomalies are influenced by the wind; they are and the wind-induced component is of atmospheric origin. But the gradient-induced component can be generated by the ocean if anomalous specific humidity differences across the air–sea boundary are dominated by saturated specific humidity anomaly at the sea surface (Kraus and Morrison 1966). So D. Cayan (1998, personal communication) kindly provided us with the gradient-induced part of latent heat flux anomalies from the Comprehensive Ocean–Atmosphere Data Set (COADS) (Slutz et al. 1985; Woodruff et al. 1993), and we correlated it with SST anomalies, both datasets filtered on interannual timescales from 1984 to 1998 (Fig. 7), with period chosen to coincide with that associated with robust coupled Rossby waves (Fig. 6). We find the anomalous gradient-induced component of latent heat flux positively correlated with SST anomalies in the eastern and central south Indian Ocean, maximum (>0.7) in the eastern ocean, decreasing to negative correlation in the western ocean. This means that interannual SST anomalies in the Indian Ocean are capable of forcing the overlying atmosphere in the eastern and central ocean, with the wind-induced latent heat flux component presumably providing a feedback to the ocean.

The expression in Eq. (9.1) approximates the influence that pycnocline depth anomalies (h) associated with interannual Rossby waves have upon SST anomalies (T) through anomalous entrainment, consistent with observed phase relationships discussed in section 6. We excluded in this idealized heat budget other terms like the horizontal advection of the background temperature distribution by the anomalous geostrophic currents associated with the Rossby waves because they produce an anomalous SST tendency that puts SST and SLH anomalies 90° out of phase from one another. This is inconsistent with the observations. We have also excluded the horizontal advection of SST anomalies by other mean and variable currents (i.e., the background mean flow and anomalous Ekman flow) because they do not derive from Rossby waves. These other terms have been shown (e.g., Wang and Weisberg 1996) to be responsible for slow coupled SST waves propagating in both the eastward and westward directions depending upon the combination of mean heat advection, anomalous Ekman heat advection, wind-induced latent heat flux anomalies, and wind-induced entrainment anomalies. Here we seek to isolate the coupled Rossby wave physics, establishing whether they are capable of producing phase speeds similar to those observed (right, Fig. 3).

For SLH anomalies of order 0.02 m (left, Fig. 3) we expect pycnocline depth anomalies (h) to be of order 5 m through the steric effect (i.e., with $SLH = (\rho'/\rho)h$ where $(\rho'/\rho) = 2.5 \times 10^{-3}$). With \bar{H} approximately 250 m and $K_H/K_T = 0.5$, then a pycnocline depth anomaly of approximately 5 m in Eq. (9.1) yields an SST anomaly of approximately 0.2°C as observed (left, Fig. 3).

To establish how SST anomalies influence the overlying atmosphere we refer the reader to the appendix of White et al. (1998) where SST-induced midtroposphere diabatic heating anomalies are assumed to be in balance with anomalous vertical heat advection in order to conserve potential temperature, yielding low-level convergence anomalies. These SST-induced low-level convergence anomalies in turn are assumed to be in balance with anomalous meridional advection of planetary vorticity in order to conserve potential vorticity. These physics have been discussed in detail by Palmer and Sun (1985). They yield the following relationships between SST (T) and MSW (v_A) anomalies:

$$v_A = (f\alpha)/(\beta C_A^2)T, \quad (9.2)$$

where f represents the Coriolis parameter, β represents the meridional derivative of the Coriolis parameter, α represents a proportionality constant relating SST anomalies to midtroposphere diabatic heating anomalies, and C_A represents the internal wave speed of the troposphere. This expression in Eq. (9.2) yields the influence that SST anomalies (T) associated with oceanic Rossby waves have upon the anomalous MSW (v_A) anomalies, consistent with observed phase relationships established in section 6.

The feedback from atmosphere to ocean operates through anomalous WSC forcing of the wind-driven Rossby wave equation, which can be written in the following form:

$$\partial v_o/\partial t + C_R \partial v_o/\partial x = -(\gamma g'/f^2)[\nabla^2 v_A - (\beta/f)\partial v_A/\partial y], \quad (9.3)$$

where v_o is the meridional geostrophic current anomaly [i.e., $v_o = (g'/f)\partial h/\partial x$]; C_R is the westward phase speed for free oceanic Rossby waves, with real world estimates given by Killworth et al. (1997); g' is reduced gravity (i.e., $g\rho'_0/\rho_0$); ρ'_0 is the density difference between the upper layer of the ocean and the deep ocean. The perturbation expansion allows us to relate the bulk formula for wind stress components linearly to anomalous zonal and meridional surface wind components (u_A and v_A , respectively) via a coefficient γ , the latter equal to the product of the mean surface wind speed, the drag coefficient, and the ratio of air density to water density, keeping the wind speed in γ equal to a constant. Since WSC anomalies respond to the rotational component of the anomalous wind only, we can relate $\partial v_A/\partial y = -$

$\partial u_A/\partial x$ in the lower troposphere and represent anomalous WSC forcing on the rhs of Eq. (9.3) in terms of MSW (v_A) anomalies.

Individual equations in Eqs. (9.1)–(9.3) form a set that together describes the simple physics of coupled Rossby waves in the Indian Ocean. These equations, relating atmosphere to ocean and ocean to atmosphere, are qualitatively consistent with observed phase relationships between spatial patterns of anomalous oceanic and atmospheric variables discussed in section 6. This set of equations reduces easily to one equation in one unknown by relating v_A in the wind-forced oceanic Rossby wave equation in Eq. (9.3) to SST anomalies in Eq. (9.2) yielding

$$\begin{aligned} \partial v_o/\partial t + C_R \partial v_o/\partial x \\ = -(A_o g'/f)[\nabla^2 T + (\beta/f)\partial T/\partial y - (\beta/f)^2 T], \end{aligned} \quad (9.4)$$

where $A_o = (\gamma\alpha)/(\beta C_\lambda^2)$ captures the various parameters already discussed in connection with Eqs. (9.1)–(9.3), with γ , α , β , g' , and C_λ^2 assumed to be constant for the sake of simplicity. We can complete this reduction process by allowing anomalous T in Eq. (9.4) to be related to anomalous SLH in Eq. (9.1) and using geostrophy, yielding

$$\begin{aligned} \partial^2 h/\partial t \partial x + [C_R + A\bar{T}/\bar{H}]\partial^2 h/\partial x^2 + [A\bar{T}/\bar{H}]\partial^2 h/\partial y^2 \\ + A[\nabla^2(\bar{T}/\bar{H}) + (\beta/f)\partial(\bar{T}/\bar{H})/\partial y - (\beta/f)^2(\bar{T}/\bar{H})]h \\ + A[2\partial(\bar{T}\bar{H})/\partial y + (\beta/f)\bar{T}\bar{H}]\partial h/\partial y \\ + A[2\partial(\bar{T}\bar{H})/\partial x]\partial h/\partial x = 0, \end{aligned} \quad (9.5)$$

where $A = A_o K_H/K_T = \gamma\alpha K_H/(\beta C_\lambda^2 K_T)$. This coupled Rossby wave equation is different from the free Rossby wave equation, given by the lhs of Eq. (9.3) = 0. The coupled Rossby wave equation introduces new phase speeds and the possibility for growth capable of maintaining the amplitudes of coupled waves against dissipation.

We can begin to understand how coupling alters the westward phase speed of free oceanic Rossby waves by assuming these phase speeds to be represented by spatial-averaged values over the Indian Ocean. This allows us to assume a wave form for h of $\exp(kx + \lambda y - \sigma t)$ in Eq. (9.5), yielding the following dispersion relation:

$$\begin{aligned} \sigma = (C_R + A\bar{T}/\bar{H})k + (A\bar{T}/\bar{H})(\lambda/k)\lambda \\ - (A/\bar{H})[\nabla^2 \bar{T} + (\beta/f)\partial \bar{T}/\partial y - (\beta/f)^2 \bar{T}]k^{-1} \\ - i[(A/\bar{H})(2\partial \bar{T}/\partial y + (\beta/f)\bar{T})\lambda + (A/\bar{H})(2\partial \bar{T}/\partial x)]k^{-1} \\ = 0, \end{aligned} \quad (9.6)$$

where we have simplified the expression by taking \bar{H} to be constant. In this expression, σ is complex frequency and (k, λ) are real zonal and meridional wavenumber components, respectively, for the coupled wave. The zonal phase speed is

$$\begin{aligned} \sigma/k = C_R + C_{CX} + C_{CX}(\lambda/k)^2 \\ - C_{CX}[(1/\bar{T})\nabla^2 \bar{T} + (\beta/f)(1/\bar{T})\partial \bar{T}/\partial y \\ - (\beta/f)^2]k^{-2}, \end{aligned} \quad (9.7)$$

where $C_{CX} = A(\bar{T}/\bar{H})$. Thus coupling can be seen to introduce positive eastward phase speed components acting to reduce the negative westward phase speed of free Rossby waves. We demonstrate this by computing the various zonal phase speed contributions on the rhs of Eq. (9.7) from the distribution of \bar{T} computed from available NCEP SST data for 29 years from 1970 to 1998 (bottom, Fig. 8). We evaluate A with constants taken from White et al. (1998): that is, $\gamma = 1 \times 10^{-5} \text{ m s}^{-1}$; $\alpha = 2 \times 10^{-3} \text{ m}^2 \text{ s}^{-3} (\text{°C})^{-1}$; $g' = 0.03 \text{ m s}^{-2}$; $\beta = 2.0 \times 10^{-11} \cos(\theta) \text{ m}^{-1} \text{ s}^{-1}$; $C_\lambda^2 = 10^3 \text{ m}^2 \text{ s}^{-2}$. We

choose $\bar{H} = 250$ m and $K_H/K_T = 0.5$ as discussed in connection with [Eq. \(9.1\)](#). We estimate $k = 2\pi/(5 \times 10^6)$ m⁻¹ and $\lambda = 2\pi/(10 \times 10^6)$ m⁻¹ from zonal and meridional spacescales in [Fig. 4](#) and [Fig. 5](#).

We plot the coupling phase speed contributions on the rhs of [Eq. \(9.7\)](#) (top, [Fig. 8](#)): the positive second and third terms can be seen to reduce the negative phase speed of the free waves, as does the sum of negative fifth and positive sixth terms; contributions from the fourth term depending upon the Laplacian of the mean SST distribution are negligible. The net contribution from the coupling phase speed components reduces the free Rossby wave speed C_R to values in the range of those observed of coupled Rossby waves (top, [Fig. 8](#)). The meridional profile of the net westward coupling speed, with magnitudes $\frac{1}{3}$ to $\frac{1}{2}$ of free wave speeds, may not look much different from those of second-mode baroclinic Rossby waves ([Pedlosky 1996](#), pp. 107–113), but the latter would not be expected to propagate westward in fixed phase with covarying SST and MSW anomalies as observed in this study.

These coupled Rossby waves are stable or growing when the imaginary term in the dispersion relation [[Eq. \(9.6\)](#)] is set to zero or some positive value, respectively, requiring meridional as well as zonal phase propagation. Stable coupled waves require the ratio of meridional wavenumber λ to zonal wavenumber k be the following:

$$\lambda/k = -(\partial\bar{T}/\partial x)/[\partial\bar{T}/\partial y + 0.5(\beta/f)\bar{T}]. \quad (9.8)$$

The mean SST distribution (bottom, [Fig. 8](#)) yields scale estimates for $\partial\bar{T}/\partial x$, $\partial\bar{T}/\partial y$, and $0.5(\beta/f)\bar{T}$ in the middle of our region of interest ([Fig. 1](#)) at 18°S of approximately -1×10^{-7} , $+5 \times 10^{-6}$, and -5×10^{-6} °C m⁻¹, respectively. Thus the magnitude of both numerator and denominator on the rhs of [Eq. \(9.8\)](#) are of order 1×10^{-7} °C m⁻¹, in which case λ is on the same order as k but of indeterminate sign. Farther poleward at 25°S, numerator and denominator are approximately -5×10^{-7} and $+1 \times 10^{-6}$ °C m⁻¹, respectively, in which case $\lambda = 0.5k$, with westward propagating waves directed poleward with meridional wavelengths similar to those observed ([Fig. 4](#) and [Fig. 5](#)). Farther equatorward at 10°S, numerator and denominator are approximately $+1 \times 10^{-7}$ and -2×10^{-6} °C m⁻¹, respectively, in which case $\lambda = 0.1k$, with westward propagating waves directed poleward but with meridional wavelengths so long that wave crests make an angle with the meridian of only 6°.

10. Discussion and conclusions

In the present study we examine the ocean–atmosphere coupling of Rossby waves in the Indian Ocean from 10°S to 30°S on interannual period scales ranging from 2 to 5 yr. Initially we examine westward phase propagation between covarying SLH, SST, MSW anomalies during the availability of T–P altimetry for 6 years from 1993 to 1998, examining the phase relationships between the three variables. Over these 6-yr time sequences the anomalies were low-pass filtered for interannual signal >2 yr allowing only 1 to 2 cycles of variability to be observed. In the absence of T–P SLH data we examine the westward phase propagation of covarying SST and MSW anomalies from 1970 to 1998 in the NCEP reanalysis, establishing the existence of coupled Rossby waves on interannual timescales over the 29 years. In both the shorter 6-yr record and the longer 29-yr record coupled Rossby waves were present, weak, or absent during different periods, consistent with a similar intermittence observed for tropical coupled Rossby wave in the Pacific Ocean ([White 2000](#)). Here we establish that coupled waves were superimposed upon standing waves in the Indian Ocean, which in the longer 29-yr record were able to be partitioned from one another using CEOF analysis. We found the standing wave dominating the propagating wave on occasion, but over most of the record the propagating wave could be discerned.

In the shorter 6-yr record the coupled Rossby wave intensity depended upon the degree of alignment among the SLH, SST, and MSW anomalies, with better alignment during the second half of the record than during the first half. In the longer 29-yr record we partitioned standing and propagating waves in SST and MSW anomalies, finding coupled Rossby wave activity nearly always present, but during some years dominated by standing wave activity. During the period from 1986 to 1990 when [Perigaud and Delecluse \(1993\)](#) observed SLH and WSC anomalies taking 2–3 years to transit the Indian Ocean, we also observe SST and MSW anomalies taking 2–3 years to make the transit, but this occurred faster than the 3 to 4 years required over most of the record.

When coupled Rossby waves were robust their westward phase speeds were less than expected of free Rossby waves, decreasing from 0.07 to 0.04 m s⁻¹ from 10°S to 30°S, respectively. Consistent with this, they displayed a weaker version of the beta refraction pattern typical of free Rossby waves ([White 1977](#)). This may also have occurred in response to a stability requirement found in the simple coupled model, which has coupled waves propagating weakly poleward in order to maintain their amplitude against dissipation.

The physics of the coupling between ocean and atmosphere is reflected in the phase relationships among interannual SLH,

SST, and MSW anomalies. Coherence and phase information yielded the same phase relationship between SST and MSW anomalies as observed in the extratropical Pacific Ocean (White et al. 1998), where poleward MSW anomalies appeared to be in equilibrium with warm SST anomalies so as to conserve potential vorticity in response to anomalous SST-induced vortex stretching of the lower troposphere (Palmer and Sun 1985). But the phase relationship between SLH and SST anomalies in the Indian Ocean was very different than in the Pacific Ocean, where warm SST anomalies were observed displaced approximately 90° of phase to the west of high SLH anomalies. In the south Indian Ocean, warm (cool) SST and high (low) SLH anomalies were approximately aligned. The latter suggests that the anomalous heat loss by the upper ocean to the lower troposphere through sensible-plus-latent heat exchange is balanced by an anomalous heat gain by reducing the entrainment of cold water into the near-surface mixed layer during autumn–winter through anomalous deepening of the main pycnocline (Moisan and Niiler 1998).

Inferring these thermodynamical processes from the phase relationships between SLH, SST, and MSW anomalies allowed us to construct a simple analytic model for coupled Rossby waves in the Indian Ocean. This model is useful in establishing whether the proposed coupling mechanisms can reduce the westward phase speeds associated with free Rossby waves to those observed. It yields a dispersion relation with phase speeds in qualitative agreement with observations. The model produces westward phase speeds ranging from 0.01 at 26°S to 0.14 m s^{-1} at 10°S , slower than expected of free Rossby waves by factors of 2 and 3 but with a wider range than observed (i.e., from 0.04 at 26°S to 0.07 m s^{-1} at 10°S). Model wave amplitude is maintained for coupled waves traveling westward and poleward, as observed. This model represents a different class of coupled Rossby waves from those constructed for coupled waves in the Pacific ocean (White et al. 1998; White 2000). Yet the proposed influence of Rossby wave activity on near-surface mixed layer thermodynamics will need to be verified by diagnosing the upper-ocean heat budget in a coupled ocean–atmosphere model capable of simulating these coupled Rossby waves in the Indian Ocean.

Finally, we illustrate how coupling in this simple analytic model works to produce westward phase speeds slower than free Rossby wave speeds (Fig. 9). This illustration begins with a wave pattern in SLH anomaly (η) propagating westward across the Indian Ocean (Fig. 9, top) with a refraction pattern similar to that observed (Fig. 4 and Fig. 5). Here positive (negative) pycnocline depth anomalies (h) produce positive (negative) SLH anomalies and positive (negative) SST anomalies directly above; thus, warm (cool) SST anomalies are aligned with high (low) SLH anomalies as observed (left, Fig. 3). Now this illustration moves to the bottom panel of Fig. 9 where poleward (equatorward) MSW and eastward (westward) zonal surface wind anomalies overlie warm (cool) SST anomalies as observed (left, Fig. 3). Consistent with the linearized surface wind stress anomaly in Eq. (9.3), anticyclonic (cyclonic) WSC anomalies (i.e., $\partial v_A/\partial x - \partial u_A/\partial y$) are displaced 90° of phase to the east of high (low) SLH anomalies and warm (cool) SST anomalies. This anticyclonic (cyclonic) WSC anomaly drives anomalous downwelling (upwelling) Ekman pumping (i.e., $\partial h/\partial t$) consistent with Eq. (9.3), yielding an eastward coupled phase speed that retards the westward phase speed of the free Rossby waves.

Acknowledgments

Warren White is supported by the National Aeronautics and Space Administration under Contract NA27GPO-539, by the Office of Global Programs of the National Oceanic and Atmospheric Administration (NOAA NA 47GP0-188) in concert with the Scripps–Lamont Consortium on the Ocean’s Role in Climate, by the National Science Foundation (OCE-9401514) in concert with the World Ocean Circulation Experiment. Support also is given by the Scripps Institution of Oceanography of the University of California, San Diego. I thank Dan Cayan for allowing me to use his partition of COADS latent heat flux anomalies into gradient-induced and wind-induced components. I thank programmers Ted Walker and Jeffrey Annis for their efforts in conducting analyses utilized in this study, and I appreciate the efforts of Andrea Fincham in preparing the final figures.

REFERENCES

- Bendat, J. S., and A. G. Piersol, 1986: *Random Data: Analysis and Measurement Procedures*. John Wiley and Sons, 566 pp.
- Chatfield, C., 1989: *The Analysis of Time Series: An Introduction*. Chapman and Hall, 241 pp.
- Frankignoul, C., and R. W. Reynolds, 1983: Testing a dynamic model for mid-latitude sea surface temperature. *J. Phys. Oceanogr.*, **13**, 1131–1145. [Find this article online](#)
- Gill, A. E., 1980: Some simple solutions for heat induced tropical circulation. *Quart. J. Roy. Meteor. Soc.*, **106**, 447–462.
- Jackson, L. B., 1996: *Digital Filters and Signal Processing*. Kluwer Academic Publishers, 502 pp.
- Jenkins, G. M., and D. G. Watts, 1968: *Spectral Analysis and its Applications*. Holden-Day, 502 pp.

- Kalnay, E., and Coauthors, 1996: The NCEP/NCAR 40-Year Reanalysis Project. *Bull. Amer. Meteor. Soc.*, **77**, 437–471. [Find this article online](#)
- Kaylor, R. E., 1977: Filtering and decimation of digital time series. Tech. Rep. Note BN 850, Institute for Physical Science and Technology, University of Maryland at College Park, 14 pp. [Available from Institute for Physical Science and Technology, University of Maryland at College Park, College Park, MD 20742-3281.].
- Killworth, P. D., D. B. Chelton, and R. A. deZoeke, 1997: The speed of observed and theoretical long extra-tropical planetary waves. *J. Phys. Oceanogr.*, **27**, 1946–1966. [Find this article online](#)
- Kraus, E. B., and R. E. Morrison, 1966: Local interactions between the sea and the air at monthly and annual time scales. *Quart. J. Roy. Meteor. Soc.*, **92**, 114–127.
- Masumoto, Y., and G. Meyers, 1998: Forced Rossby waves in the southern tropical Indian Ocean. *J. Geophys. Res.*, **103**, 27 589–27 602.
- Moisan, J. R., and P. P. Niiler, 1998: The seasonal heat budget of the North Pacific: Net heat flux and heat storage rates (1950–1990). *J. Phys. Oceanogr.*, **28**, 401–421. [Find this article online](#)
- Palmer, T. N., and Z. Sun, 1985: A modeling and observational study of the relationship between sea surface temperature in the north-west Atlantic and the atmospheric general circulation. *Quart. J. Roy. Meteor. Soc.*, **111**, 947–975.
- Pedlosky, J., 1996: *Ocean Circulation Theory*. Springer Verlag, 453 pp.
- Perigaud, C., and P. Delecluse, 1993: Interannual sea level variations in the tropical Indian Ocean from Geosat and shallow-water simulations. *J. Phys. Oceanogr.*, **23**, 1916–1934. [Find this article online](#)
- Preisendorfer, R. W., 1988: *Principal Component Analysis in Meteorology and Oceanography*. Elsevier, 425 pp.
- Reynolds, R. W., and D. C. Marsico, 1993: An improved real-time global sea surface temperature analysis. *J. Climate*, **6**, 114–119. [Find this article online](#)
- Slutz, R. J., S. J. Lubker, J. D. Hiscox, S. D. Woodruff, R. L. Jenne, D. H. Joseph, P. M. Steurer, and J. D. Elms, 1985: Comprehensive Ocean–Atmosphere Data Set; Release 1. NOAA/Environmental Research Laboratory, 268 pp.
- Snedecor, G. W., and W. G. Cochran, 1980: *Statistical Methods*. Iowa State University Press, 507 pp.
- von Storch, H., and F. W. Zwiers, 1999: *Statistical Analysis in Climate Change Research*. Cambridge University Press, 484 pp.
- Wang, C., and R. H. Weisberg, 1996: Stability of equatorial modes in a simplified coupled ocean–atmosphere model. *J. Climate*, **9**, 3132–3148. [Find this article online](#)
- White, W. B., 1977: Annual forcing of baroclinic long waves in the tropical North Pacific. *J. Phys. Oceanogr.*, **7**, 50–61. [Find this article online](#)
- , 2000: Tropical coupled Rossby waves in the Pacific Ocean–atmosphere system. *J. Phys. Oceanogr.*, **30**, 1245–1264. [Find this article online](#)
- , and J. F. T. Saur, 1983: Sources of interannual baroclinic waves in the eastern subtropical North Pacific. *J. Phys. Oceanogr.*, **13**, 1035–1046. [Find this article online](#)
- , and D. R. Cayan, 2000: A global ENSO wave in surface temperature and pressure and its interdecadal variability from 1900 to 1996. *J. Geophys. Res.*, **105**, 11223–11242.
- , Y. Chao, and C.-K. Tai, 1998: Coupling of biennial oceanic Rossby waves with the overlying atmosphere in the Pacific basin. *J. Phys. Oceanogr.*, **28**, 1236–1251. [Find this article online](#)
- Woodruff, S. D., S. J. Lubker, K. Wolter, S. J. Worley, and J. D. Elms, 1993: Comprehensive Ocean–Atmosphere Data Set Release 1a; 1980–92. *Earth Syst. Monitor*, **4**, 1–8.

APPENDIX

11. Methods of Filtering

a. General method of digital filtering

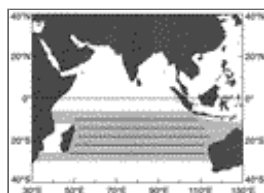
We designed a nonrecursive finite impulse response (FIR) filter based on Kaiser's window (Jackson 1996, pp. 296–301). Half-power points of “A” and “B” cycles per sample were used to define the bandpass filter. The number of Kaiser weights for the filter (giving the filter width) was then chosen to acquire the desired frequency response function, which is the discrete Fourier transform of the filter's impulse response (bottom right, Fig. A1). For a FIR of P elements (Kaiser weights) the N element time or space sequence is extended by $P/2$ samples on either side (backcast/forecast) using a $(N - 1)$ th order autoregressive model (Chatfield 1989, 35–40). Then, the FIR was convolved with the extended time or space sequence. The nonextended portion (N samples) of this filtered sequence was then extracted to represent the filtered record.

b. Temporal filtering of monthly SLH, SST, and MSW anomalies

We conducted this temporal filtering procedure with three steps. First, we calculated monthly anomalies for the 72-month time sequence (January 1993–December 1998). Second, using the general principles given above, we designed a lowpass FIR filter with half-power point at $1/24$ cycles per month. The FIR had 28 elements (Kaiser weights). Third, the 72-month time sequence was extended by 30 months on either end (backcast/forecast) using a 71th order autoregressive model. Finally, the FIR filter was convolved with the extended time sequence and the nonextended portion (72 months) of the filtered sequence extracted to represent the temporally filtered time sequence (bottom left, Fig. A1).

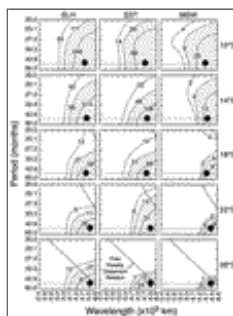
A Monte Carlo simulation using red noise demonstrates that this extension/filtering method yields errors in the filtered 72-month time sequences near both ends (top, Fig. A1). We constructed time sequences of filtered red noise of practically unlimited length (i.e., the reference signal) for comparison with that of the extended and filtered red noise time sequence of 72-month duration (i.e., the extended signal). Then we differenced the reference and extended signals over 5000 realizations. We find the root mean square (rms) estimates of these differences to be less than 25% for months 7 to 66 over the 72-month time sequence, extending over the 60 months in the interior portion of the record. So, for the present study we chose to analyze the 60 months from July 1993 to July 1998 in the middle of the 72-month record extending from January 1993 to December 1998.

Figures



Click on thumbnail for full-sized image.

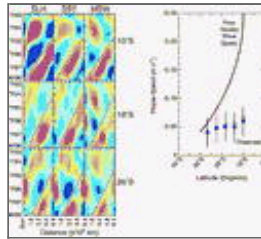
Fig. 1. Map of the Indian Ocean showing the shaded region of interest where anomalies of T–P sea level height (SLH), NCEP sea surface temperature (SST), and meridional surface wind (MSW) are examined. Zonal lines at 4° lat increments from 10°S to 26°S lat define longitudes along which monthly SLH, SST, and MSW anomalies are analyzed with spectral methods. These zonal lines extend over 65° of longitude, corresponding to 6400 km



Click on thumbnail for full-sized image.

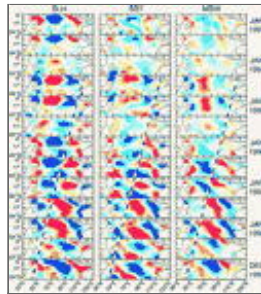
Fig. 2. Propagation zonal wavenumber–frequency spectra (Bendat and Piersol 1986, pp. 361–424) of interannual SLH, SST, and MSW anomalies along 10° , 14° , 18° , 22° , and 26° lat in the Indian Ocean, computed from time–longitude diagrams along zonal lines in Fig. 1 over the 60 months from Jul 1993 to Jun 1998. Spectral energy densities are contoured at $10^2 \text{ m}^2/(\text{s}^{-1} \text{ m}^{-1})$ for SLH, $10^4 \text{ }^\circ\text{C}^2/(\text{s}^{-1} \text{ m}^{-1})$ for SST, and $10^5 (\text{m s}^{-1})^2/(\text{s}^{-1} \text{ m}^{-1})$ for MSW. Contours are significantly different from adjacent contours at the 90% confidence level (Jenkins and Watts 1968, pp. 77–89). Hatched lines are for effect. Solid circles show wavenumber–

frequency bands of shared peak spectral energy density among the three spectra at each latitude. Sloping lines delineate free Rossby wave dispersion curves computed by [Killworth et al. \(1997\)](#). Thin horizontal lines indicate the period of 48 months



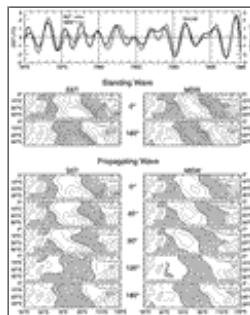
[Click on thumbnail for full-sized image.](#)

Fig. 3. (left) Time-longitude diagrams for interannual SLH, SST, and MSW anomalies at 10°S, 18°S, and 26°S in the Indian Ocean over longitudes given by zonal lines in [Fig. 1](#), extending over 60 months from Jul 1993 to Jun 1998. Negative (positive) anomalies range from blue to purple (yellow to red) at intervals of 0.005 m for SLH anomalies, 0.05°C for SST anomalies, and 0.1 m s⁻¹ for MSW anomalies. Dashed lines in these time-longitude diagrams are provided for reference. (right) Meridional profile of westward phase speeds for interannual SLH anomalies (closed circles) referenced to theoretical speeds for free Rossby waves (solid line) computed by [Killworth et al. \(1997\)](#). Observed westward phase speeds were computed from slopes of dashed lines in time-longitude diagrams extending from 1993 to 1998 (left, [Fig. 3](#)), with error bars representing estimated variation taking into account errors in interannual SLH anomalies. Westward phase speeds are also displayed for covarying interannual SST and MSW anomalies (open circles) in time-longitude diagrams extending from 1970 to 1998 (e.g., [Fig. 6](#))



[Click on thumbnail for full-sized image.](#)

Fig. 4. Animation sequence of maps for interannual SLH, SST, and MSW anomalies. Negative (positive) SLH and SST anomalies and polward (equatorward) MSW anomalies range from blue to purple (yellow to red) with contour intervals of 0.005 m for SLH anomalies, 0.05°C for SST anomalies, and 0.05 m s⁻¹ for MSW anomalies. Dashed lines provide reference. The sense of propagation comes from following anomalies of similar sign from one map to the next in each animation sequence of maps



[Click on thumbnail for full-sized image.](#)

Fig. 5. (top) Time sequences of the real component of the first CEOF modes of interannual SST and MSW anomalies computed over the Indian Ocean for 29 years from 1970 to 1998. (middle) Animation sequences of maps displaying the weights of the standing waves in the first CEOF modes, with each map extending across the Indian Ocean from 0° to 35°S. Only peaks and troughs of the standing waves are shown at 0° and 180° of phase. (bottom) Same as above but for propagating waves in the first CEOF modes, extending over ½ cycle from 0° to 180° of phase in 45° increments (see text for details). The sense of propagation comes from following weights of similar sign from one map to the next. Unshaded (shaded) regions indicate positive (negative) weights, with contours at intervals of 0.025°C for SST and 0.1 m s⁻¹ for MSW



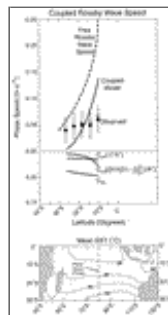
Click on thumbnail for full-sized image.

Fig. 6. (top left) Time–longitude diagrams of interannual SST and MSW anomalies extending across the Indian Ocean from 50° to 110°E, averaged from 14°S to 18°S for 29 years from 1970 to 1998. (top right) Same as at left but for reconstructed SST and MSW anomalies from the propagating wave component in the first CEOF mode (see text for details). Negative (positive) anomalies are hatched (unhatched). Gray sloping lines indicate the speed of westward phase propagation and allow assessment of the alignment between the two variables. Contours intervals are 0.1°C and 0.2 m s⁻¹. (bottom) Average zonal lag cross-correlations between interannual SST and MSW anomalies for two halves of the record, with 90% confidence limits of 0.35 given by the horizontal dashed lines for 20 effective degrees of freedom ([Snedecor and Cochran 1980](#))



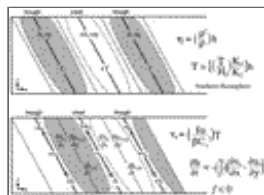
Click on thumbnail for full-sized image.

Fig. 7. Distribution of cross correlations at zero time lag between interannual SST anomalies and interannual latent heat flux anomalies from 1982 to 1998, the latter containing only the gradient-induced part (Q_{EE}) associated with anomalous air–sea specific humidity differences. Positive (negative) correlation are unhatched (hatched), with values greater than 0.48 significant at the 90% confidence level for 12 effective degrees of freedom ([Snedecor and Cochran 1980](#))



Click on thumbnail for full-sized image.

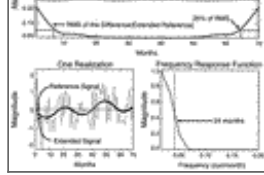
Fig. 8. (top) Meridional profiles of zonal phase speeds for model coupled Rossby waves and their various contributions (see text for further details). Also displayed are observed westward phase speeds for interannual SLH anomalies (closed and open circles) and the theoretical speeds for free Rossby waves (dashed line) computed by [Killworth et al. \(1997\)](#), both repeated from [Fig. 3](#). Model westward phase speeds were computed from Eq. (8.7) in the text. (bottom) Distribution of annual mean SST over the Indian Ocean from 0° to 30°S, computed from NCEP reanalysis for the 29 years from 1970 to 1998 ([Reynolds and Marsico 1993](#))



Click on thumbnail for full-sized image.

Fig. 9. Schematic diagram illustrating how ocean and atmosphere in the Indian Ocean are coupled in order to reduce the westward phase speed of free Rossby waves. Equations at right govern kinematic and dynamical relationships between variables, while diagrams at left display spatial phase relationships estimated from coherence and phase information. (top) High (low) SLH anomalies [η] generate warm (cool) SST anomalies (T) through the anomalous downward (upward) displacement of the main pycnocline (h) influencing anomalous entrainment of colder deeper water into the near-surface mixed layer during autumn–winter. Light (dark) shading indicates where η , h , and T are positive (negative). (bottom) MSW anomalies (v_A) and ZSW (u_A) anomalies come into balance with underlying SST anomalies through the latter’s influence upon midtroposphere diabatic heating, the zonal gradient of which yields WSC anomalies [$\text{curl}(\tau/(\rho_O)) \approx (\gamma/f)(\partial v_A/\partial x - \partial u_A/\partial y)$]. The WSC anomalies generate anomalous Ekman pumping ($\partial h/\partial t$) of oceanic Rossby waves. Light (dark) shading indicates where $(\partial v_A/\partial x - \partial u_A/\partial y)$ and $\partial h/\partial t$ are positive (negative); arrows along wave crests indicate the direction of the MSW and ZSW anomalies that overlie wave crests and troughs. Unshaded regions in the bottom panel mark the positive SLH tendency anomaly [$\partial \eta/\partial t$] displaced eastward of unshaded regions in the upper panel marking positive SLH anomaly [η], yielding eastward phase propagation due to coupling, which decreases the westward phase propagation of free Rossby waves





Click on thumbnail for full-sized image.

Fig. A1. Discussion of the figure is in text of the appendix

Corresponding author address: Warren B. White, Physical Oceanography Research Division, Scripps Institution of Oceanography, 9500 Gilman Drive, La Jolla, CA 92093-0230.

E-mail: wwhite@ucsd.edu

top ▲



© 2008 American Meteorological Society [Privacy Policy and Disclaimer](#)
Headquarters: 45 Beacon Street Boston, MA 02108-3693
DC Office: 1120 G Street, NW, Suite 800 Washington DC, 20005-3826
amsinfo@ametsoc.org Phone: 617-227-2425 Fax: 617-742-8718
[Allen Press, Inc.](#) assists in the online publication of AMS journals.